



Full length article

Implant degradation of low-alloyed Mg–Zn–Ca in osteoporotic, old and juvenile rats



Nicole G. Sommer^a, Daniela Hirzberger^a, Lisa Paar^a, Leopold Berger^b, Hanna Ćwieka^c, Uwe Y. Schwarze^{a,d}, Valentin Herber^{a,d}, Begüm Okutan^a, Andrew J. Bodey^e, Regine Willumeit-Römer^c, Berit Zeller-Plumhoff^c, Jörg F. Löffler^b, Annelie M. Weinberg^{a,*}

^a Department of Orthopedics and Traumatology, Medical University of Graz, 8036, Graz, Austria

^b Laboratory of Metal Physics and Technology, Department of Materials, ETH Zurich, 8093, Zurich, Switzerland

^c Institute of Metallic Biomaterials, Helmholtz-Zentrum hereon GmbH, 21502, Geesthacht, Germany

^d Department of Dentistry and Oral Health, Division of Oral Surgery and Orthodontics, Medical University of Graz, 8010, Graz, Austria

^e Diamond Light Source Ltd., Harwell Science and Innovation Campus, Didcot, Oxfordshire, OX11 0DE, UK

ARTICLE INFO

Article history:

Received 31 January 2022

Revised 27 April 2022

Accepted 23 May 2022

Available online 27 May 2022

Keywords:

Magnesium-based implants

Osteoporosis

Degradation

Histology

Micro-computed tomography

Synchrotron radiation

ABSTRACT

Implant removal is unnecessary for biodegradable magnesium (Mg)-based implants and, therefore, the related risk for implant-induced fractures is limited. Aging, on the other hand, is associated with low bone-turnover and decreased bone mass and density, and thus increased fracture risk. Osteoporosis is accompanied by Mg deficiency, therefore, we hypothesized that Mg-based implants may support bone formation by Mg²⁺ ion release in an ovariectomy-induced osteoporotic rat model. Hence, we investigated osseointegration and implant degradation of a low-alloyed, degrading Mg–Zn–Ca implant (ZX00) in ovariectomy-induced osteoporotic (Osteo), old healthy (OH), and juvenile healthy (JH) groups of female Sprague Dawley rats via *in vivo* micro-computed tomography (μ CT). For the Osteo rats, we demonstrate diminished trabecular bone already after 8 weeks upon ovariectomy and significantly enhanced implant volume loss, with correspondingly pronounced gas formation, compared to the OH and JH groups. Sclerotic rim development was observed in about half of the osteoporotic rats, suggesting a prevention from foreign-body and osteonecrosis development. Synchrotron radiation-based μ CT confirmed lower bone volume fractions in the Osteo group compared to the OH and JH groups. Qualitative histological analysis additionally visualized the enhanced implant degradation in the Osteo group. To date, ZX00 provides an interesting implant material for young and older healthy patients, but it may not be of advantage in pharmacologically untreated osteoporotic conditions.

Statement of significance

Magnesium-based implants are promising candidates for treatment of osteoporotic fractures because of their biodegradable, biomechanical, anti-bacterial and bone regenerative properties. Here we investigate magnesium–zinc–calcium implant materials in a rat model with ovariectomy-induced osteoporosis (Osteo group) and compare the related osseointegration and implant degradation with the results obtained for old healthy (OH) and juvenile healthy (JH) rats. The work applied an appropriate disease model for osteoporosis and focused in particular on long-term implant degradation for different bone conditions.

* Corresponding author: Assoc.-Prof. Dr. Annelie-Martina Weinberg, Medical University of Graz, Department of Orthopedics and Traumatology, Auenbruggerplatz 5, A-8036, Graz. Phone: 0043/316 385-78040.

E-mail addresses: nicole.sommer@medunigraz.at (N.G. Sommer), daniela.hirzberger@medunigraz.at (D. Hirzberger), lisapaar22@gmail.com (L. Paar), leopold.berger@mat.ethz.ch (L. Berger), hanna.slominska@hereon.de (H. Ćwieka), uwe.schwarze@medunigraz.at (U.Y. Schwarze), valentin.herber@medunigraz.at (V. Herber), beguem.okutan@medunigraz.at (B. Okutan), andrew.bodey@diamond.ac.uk (A.J. Bodey), regine.willumeit@hereon.de (R. Willumeit-Römer), berit.zeller-plumhoff@hereon.de (B. Zeller-Plumhoff), joerg.loeffler@mat.ethz.ch (J.F. Löffler), anneliemartina.weinberg@medunigraz.at (A.M. Weinberg).

<https://doi.org/10.1016/j.actbio.2022.05.041>

1742-7061/© 2022 The Authors. Published by Elsevier Ltd on behalf of Acta Materialia Inc. This is an open access article under the CC BY license (<http://creativecommons.org/licenses/by/4.0/>)

Enhanced implant degradation and sclerotic rim formation was observed in osteoporotic rats, which illustrates that the setting of different bone models generates significantly modified clinical outcome. It further illustrated that these differences must be taken into account in future biodegradable implant development.

© 2022 The Authors. Published by Elsevier Ltd on behalf of Acta Materialia Inc.
This is an open access article under the CC BY license (<http://creativecommons.org/licenses/by/4.0/>)

1. Introduction

Bioresorbable implants have progressively moved into the focus of materials science in recent years. Here the ideal implant material may be resorbable and reveal functionalized properties to induce and support fracture healing and remodeling. In addition, such bioresorbable implants may also be beneficial in complex situations such as osteoporosis. Due to the increased fragility rate of the bone, patients with osteoporosis run the risk of repeated bone fracture in surrounding areas [1].

Osteoporosis is a multifactorial disease that is generally subdivided into primary and secondary osteoporosis, with the latter describing osteoporosis as a secondary outcome to chronic diseases such as Cushing's syndrome [2]. In contrast, primary osteoporosis involves type 1 post-menopausal and type 2 senile osteoporosis. Type 1 post-menopausal osteoporosis is a systemic disease that is mainly driven by estrogen deficiency in women. Type 2 senile osteoporosis mainly occurs in elderly, peaks in the mid-seventies, and is overrepresented in women [3]. Type 1 and 2 primary osteoporosis affects both the cortical and trabecular bone [4,5]. Preclinical studies demonstrated a longer and more severe inflammatory phase in ovariectomy-induced osteoporotic mice with experimental bone fractures than in controls, thereby also contributing to delayed fracture healing [6].

Bone metabolism mainly depends on calcium (Ca) and Mg. Importantly, 99% of Ca in the body is stored in the skeleton and Ca homeostasis is regulated by parathyroid hormone and calcitonin [7]. Ca deficiency results in hypocalcemia ($<8.8 \text{ mg dL}^{-1}$), which is predominantly caused by vitamin-D deficiency, hypoparathyroidism and kidney diseases [8]. Hypocalcemia may lead to tetany, seizures and heart failure [9]. Importantly, Ca is known as a Mg antagonist. Various studies reported the optimal dietary intake of a 1:2 (Ca:Mg) ratio to prevent several severe outcomes, such as cancer or cardiovascular events [10,11]. Oral Ca administration has been shown to improve bone mass and density, especially in patients with osteoporosis [12,13].

However, another potential risk factor for suppression of bone mass and density as well as osteoporosis-associated fragile bone is hypomagnesemia. Mg is the fourth-most abundant mineral in the body and approximately 60% of Mg is stored in bone [14]. Epidemiological studies demonstrated a positive correlation between Mg intake and bone-mineral density [15]. Moreover, Mg-deficient diet was linked to fragile and brittle bone, trabecular microfractures and decreased cortical thickness in rat bone [16,17]. Regression analysis in postmenopausal women with and without osteoporosis revealed lower Mg levels than recommended in healthy and osteoporotic women, and Mg values also correlated with the individual bone-mineral content [18]. Animal studies revealed that osteoporosis progression is associated with dietary restriction of Mg [19]. Low to moderate Mg deficiency linked to low-grade inflammation may not only contribute to osteoporosis [20], but also to metabolic syndromes and their associated outcomes such as atherosclerosis, hypertension [21], type-2 diabetes mellitus [22] and some cancer types.

In general, osteoporosis is characterized by an imbalance of bone formation and resorption, resulting in decreased total mineralization, thereby leading to reduced bone strength and increased risk of fractures [23]. Most osteoporotic fractures occur at the trabecular or the metaphyseal bone region [24] and at locations including the distal radius, proximal humerus, proximal femur, and vertebral bodies [25,26]. During successful fracture healing, cellular and molecular events are carefully orchestrated, producing a template for regeneration and remodeling of the fracture site, followed by bone function restoration [27]. In osteoporotic bone, fracture healing is delayed and the biomechanical properties of fractured bone are decreased, thereby challenging the treatment of osteoporotic fragility fractures [28]. At a cellular level, reduced numbers and/or reduced activity of osteogenic cells (including mesenchymal stem cells and osteoblasts) are observed under osteoporotic conditions, while osteoclast activity increases. Moreover, an imbalance of anabolic and catabolic local factors has been linked to osteoporosis [23,29].

Researchers and clinicians have demonstrated delayed osseointegration of Ti and stainless steel implants under osteoporotic conditions *in vitro* and *in vivo* [30–32]. No hardware removal may thus generate late-stage infections with non-treatable outcomes, especially in situations such as osteoporosis or in elderly patients with suppressed immunity. As a potential solution, bioresorbable implant materials might overcome the disadvantages of such permanent implants used in osteosynthesis of osteoporosis-associated fragility fractures. Especially promising candidates for bioresorbable implants are Mg-based alloys, which may even be beneficial with respect to bone mineralization [33].

Only recently, we introduced a bioresorbable magnesium–zinc–calcium (MgZnCa) alloy (ZX00, with $<0.5 \text{ wt\% Zn}$ and $<0.5 \text{ wt\% Ca}$) in a pre-clinical study, using small and large juvenile growing animals, and in a first-in-men clinical trial [34–36]. The especially low amount of alloying elements (Zn and Ca) proved to be beneficial to gain exceptionally high mechanical strength and at the same time minimizing the material's degradation rate. Another previous study [37] demonstrated that Mg also supports fracture healing, especially callus formation, on a molecular level by supporting osteoinductive pathways in healthy and osteoporotic bone via neuronal secretion of calcitonin gene related polypeptide (CGRP). Substantial callus formation and an increased cortical femoral wall diameter were also observed *in vivo*, with the Mg-based implants revealing increased osteoblast activity and decreased osteoclast activity [38]. Another study reported Mg to suppress vascular smooth muscle cell calcification, in part mediated by inhibition of Wnt/ β -catenin signaling. Furthermore, Mg degradation was ascribed to attenuate osteoclast activity by inhibiting nuclear factor- κ B and NFATc1 signaling *in vitro* [39]. Accordingly, Mg-based implants exhibit several advantages and therefore provide a good alternative to treat osteoporosis-associated fragility fractures. However, since osteoporosis is divided into different subtypes and these are also categorized into different illness severity stages, the particular subtype and severity might influence the impact of such Mg-based bioresorbable implant materials. Hence, the application

of Mg-based implants in different subtypes of osteoporosis needs further detailed investigation.

In previous studies, the application of ZX00 in juvenile growing animals and in a clinical study revealed promising biocompatibility and osseointegration. Adequate gas volume formation without negative influence on bone formation and fracture healing was also observed [34–36]. Hence, in designing the present study we hypothesized that bioresorbable Mg-based implants support bone formation in untreated ovariectomy-induced osteoporotic rats due to the release of Mg^{2+} ions during the degradation process. Here, we investigated osseointegration and implant degradation of ZX00 in ovariectomy-induced osteoporotic (Osteo), old healthy (OH), and juvenile healthy (JH) Sprague Dawley rats.

2. Material and Methods

2.1. Implant production and sterilization

In a first step, Mg was purified with a custom-made distillation process [40] to such an extent that remaining impurities combined were less than 10 ppm by weight (>99.999 wt% Mg). Subsequently, this ultrahigh-purified Mg was alloyed with high-purity Zn and Ca (Zn: >99.9999wt%, Ca: >99.95wt%) under protective Ar-atmosphere to synthesize the alloy Mg <0.5wt% Zn <0.5wt% Ca (designated as ZX00). Further details on the rationale of the alloy design, processing and properties have been published elsewhere [35]. After solution- and aging-heat treatments (350°C/12h, 450°C/8h, and 250°C/30min), indirect extrusion was performed at 325°C. Subsequently, cylindrical pins ($l = 8$ mm, $d = 1.6$ mm) were machined using polycrystalline diamond tools and taking special care to avoid any kind of surface contamination. The pins were then cleaned in ethanol using ultrasonic waves, air-dried in clean-room atmosphere and packaged airtight. Sterilization was performed by gamma irradiation (minimum dose 25 kGray) [34].

2.2. Ethics statement

Animal experiments with Sprague Dawley (SD) rats were performed according to the guidelines of the legal and ethical standards, including the accommodation and care of animals, formulated by the European Convention for the Protection of Vertebrate Animals Used for Experimental and Other Scientific Purposes as well as after permission by the Austrian Federal Ministry for Science and Research. All animal experiments were carried out to minimize suffering according to the 3R principles of animal welfare – “replace, reduce and refine”. For osteoporotic studies we hold an ethical permit with the GZ number BMWFW-66.010/0124-WF/V/3b/2015.

2.3. Animals

In total, 21 female Sprague Dawley® (SD) rats, purchased from Janvier Labs (Saint Berthevin, France), were kept on normal chow diet and water *ad libidum*. All animals were housed in clear plastic cages on standard bedding under controlled conditions (12 hours/12 hours dark/light cycle). The rats were randomly divided into two main groups: (i) the skeletally mature rat group ($n=14$, housed until they reached 12 months of age) and (ii) the juvenile growing, skeletally immature, healthy rat group (JH group, $n=7$, housed until they reached 6 weeks of age). The skeletally mature rat group was further subdivided into the senile osteoporotic rat group (Osteo group) undergoing bilateral ovariectomy at the age of 12 months, and the old healthy, non-ovariectomized group (OH group), representing the aged control group. All animals received ZX00 implants. Implantation was performed at 15 months of age

for the Osteo group (3 months after ovariectomy) and for the OH group, and after 6 weeks of age for the JH group.

2.4. Ovariectomy and implantation

Anesthesia: Volatile isoflurane (Forane®, Abbot AG, Baar, Switzerland) was administered for general anesthesia preceded by a subcutaneous combined sedation, administering a mixture of Fentanyl ($20 \mu\text{g kg}^{-1}$ Fentanyl®, Janssen-Cilag GmbH, Neuss, Germany), Midazolam ($400 \mu\text{g kg}^{-1}$ Midazolam Delta®, DeltaSelect GmbH, Dreieich, Germany) and Medetomidine ($200 \mu\text{g kg}^{-1}$ Domitor®, Pfizer Corporation Austria GmbH, Vienna, Austria) via subcutaneous injection.

Antagonist and analgesia: The general anesthesia was then antagonized by an intraperitoneal injection of a mixture of Naloxone ($120 \mu\text{g kg}^{-1}$; Narcanti, Torrex Chiesi Pharma GmbH, Vienna, Austria), Flumazenil ($50 \mu\text{g kg}^{-1}$; Anexate, Roche Austria GmbH, Vienna, Austria) and Atipamezole ($250 \mu\text{g kg}^{-1}$; Antisedan, Pfizer Corporation, Vienna, Austria). Postoperatively all animals received 4 mg kg^{-1} Caprofen (Rimadyl, Pfizer Corporation, Vienna, Austria), which was injected subcutaneously on the day of operation to ensure analgesia. During the first post-operative week, analgesia was maintained by administration of 60 mg Piritramid (Dipidolor, Janssen-Cilag GmbH, Neuss, Germany) in 40 ml 5% glucose added to 500 ml drinking water. Postoperatively, the rats were allowed to move freely in their cages without external support and with unrestricted weight bearing. Observation was performed daily throughout the study period.

Ovariectomy: After disinfection, an incision was made along the middle line of the Osteo rats' respective abdomens. After complete removal of the bilateral ovaries, the rats were sutured by layer.

Transcortical implantation of ZX00 pins: All rats obtained transcortical implantation of ZX00 pins in both hind legs. These were shaved, antisepticed with alcohol pads, and dried. A skin incision with a length of 1–2 cm was made medial over the proximal lateral tibial metaphysis and bones were cleared from blood and connective tissue. A drill (1.55 mm) with ascending diameter (Synthes, Paoli, PA, USA) was used to prepare the bicortical implantation bed. Drilling was performed at a low rotational speed of 200 rpm. The cylindrical ZX00 pins were inserted by gentle tapping, resulting in a uniform press fit. After transcortical placement was ensured, the operating field was irrigated thoroughly with physiological saline solution and the wound was closed. The general anesthesia was then antagonized according to the section “ovariectomy”.

Euthanasia: All animals were euthanized with 25 mg sodium thiopental (Thiopental® Sandoz, Sandoz GmbH, Kundl, Austria) by injection into the cardiac ventricle, leading to immediate cardiac arrest [34].

2.5. In vivo micro-computed tomography (μCT)

The animals underwent *in vivo* medium-to-low resolution micro-computed tomography (μCT ; Siemens Inveon device) at 80 kV voltage, $500 \mu\text{A}$ current, and 750 ms exposure time at a resolution of $56 \mu\text{m}$. To further reduce beam hardening, a 0.5-mm aluminum filter was used for absorbing the low-energy X-rays before or after passing through the sample. The aged rats (Osteo and OH groups) underwent μCT evaluation immediately before ovariectomy (of the Osteo group), and 4, 8 and 12 weeks after the ovariectomy timepoint to observe osteoporosis progression with respect to the old healthy (OH) controls. Moreover, μCT scans were performed in all groups immediately after implantation ($t=0$) as well as 2, 6, 12, 15, 18 and 24 weeks after surgery. During the μCT examinations the animals were generally anaesthetized by volatile isoflurane (Forane®, Abbot AG, Baar, Switzerland). Three-dimensional

(3D) reconstruction was performed to quantify the implant volume, implant surface area and gas volume using MIMICS Software Version 23.0 (Materialise, Louvain, Belgium). In brief, a threshold between 226 to 3071 Hounsfield Units was placed on the images to separate implant from bone. As the prescribed thresholds of Hounsfield Units did not cover bone and implant in all μ CT images, the threshold values of Hounsfield Units had to be adjusted individually. Subsequently, the two masks were separated and manual post-processing in all planes had to be conducted in order to ensure an accurate calculation of the implant volume and surface. Subsequently, a 3D model of the implant was constructed via function „Mask - Calculate Part“ and volume (in mm^3) and surface (in mm^2) values were evaluated. Quantification of the gas volume was performed via creating a second mask with Hounsfield Units between -1000 to -1024. The threshold values were again modified individually in order to ensure a precise measurement of the entire gas volume. Via function „Mask - Calculate Part“, a 3D model of the gas volume was constructed and the gas volume in mm^3 was calculated. The obtained values for implant volume and implant surface area were subsequently used to determine the degradation rate, DR_i , similarly to previous studies [34] according the following Eq. (1):

$$\text{DR}_i = \frac{\Delta V_i}{\bar{S}_i \Delta t}, \quad (1)$$

with i the observation point, ΔV_i the volume change and \bar{S}_i the average surface area between two observation time points t_i and t_{i-1} , and Δt the difference between the two observation time points.

2.6. Ex vivo synchrotron radiation-based micro-computed tomography (SR μ CT)

To determine the relative bone volume in the implant vicinity, a small number of samples (3 JH, 3 OH, 2 Osteo) at 24 weeks of healing was imaged using SR μ CT at the Diamond Manchester Imaging Branchline I13-2 [41,42] of the Diamond Light Source synchrotron [43,44]. A polychromatic, “pink”, beam with a weighted mean photon energy of 27 keV (Pt mirror stripe; filters: 1.3 mm graphite, 3.2 mm Al) was selected for imaging off-axis around 360° with a pco.edge 5.5 CL camera (PCO AG, Kelheim, Germany). Overall, 8001 projections were acquired per tomographic scan with 80 ms exposure time and a voxel size of 1.625 μm . To cover the entire sample, several height steps were imaged per sample. The SR μ CT image data were reconstructed using the open-source Savu framework [45,46] with the TomoPy reconstruction package [47] and the application of optical distortion correction [48] and a ring-removal filter [49]. After reconstruction, the images were filtered using an iterative non-local means filter [50], binned three times and then stitched. The bone surrounding the implant was then segmented semi-automatically using region-growing and manual corrections in Amira-Avizo 2021.1 (FEI SAS, Thermo Scientific, France). The images were then aligned to an idealized initial pin (\varnothing 1.6 mm, height 8 mm), and a region of interest around the pin with a diameter enlarged by 1 mm was determined in Avizo using an Euclidian distance map. To further limit the relative bone-volume calculation to the inside of the bone, the convex hull of the segmented bone volume was determined. Within the intersection of these two regions (convex hull and enlarged pin), the relative bone-volume fraction f_{bone} = bone volume over total volume (in %) was calculated in Avizo according to [51] and following Eq. (2):

$$f_{\text{bone}} = \frac{N_{\text{bone}}}{N_{\text{tot}}}, \quad (2)$$

where N_{bone} is the number of voxels segmented as bone and N_{tot} is the number of overall voxels in the region of interest. The segmented region in the old healthy and osteoporotic group was additionally analysed for trabecular bone thickness and connectivity

using the Fiji plugin BoneJ [52]. As some cortical bone was included in the region of interest, the maximum thickness to estimate the average was limited to approx. 200 μm , by which most of the cortical bone was excluded from the analysis. The results were plotted using Jupyter Notebook (Python 3).

2.7. Histology

Extracted tibiae were cut to the region of interest and fixed in 100% ethanol to avoid further degradation of ZX00 and at the same time preserving the tissue. Ethanol was changed three times over three days to ensure dehydration, before infiltration with Technovit 9100 resin (Kulzer GmbH, 63450 Hanau, Germany) according to the user manual and final embedding in the same resin. Undecalcified thin ground sections of the regions of interests were prepared with approximately 100 μm thickness according to the Karl Donath method [53]. The sections were stained with azure I, methylene blue and basic fuchsin [54]. Digital images of the thin ground sections were obtained using a custom-made Olympus BX53 scanning system (OLYMPUS EUROPA SE & CO. KG, Hamburg, Germany).

2.8. Statistical analysis

Due to some blurred images of the *in vivo* μ CT scans, not all 14 implanted materials could be investigated in the JH group, therefore the number of samples was below 10 for this group. Nevertheless, all results are still given as mean \pm standard deviation to make them comparable between all groups and with respect to literature. Statistical analysis was performed with Graph Pad Prism version 8 (GraphPad Software, San Diego, USA). Differences between groups and time points were assessed via two-way ANOVA using the Bonferroni post-hoc test. Differences in bodyweight within a particular group were assessed *via* one-way ANOVA using the Tukey post-hoc test. A p-value <0.05 was considered statistically significant.

3. Results

3.1. Ovariectomy-induced osteoporosis progression over 12 weeks

In this study, bilateral ovariectomy was performed in 12-months old SD rats to induce osteoporosis. Osteoporosis progression was evaluated by *in vivo* low-to-medium resolution μ CT scans before ($t=0$) as well as 4, 8 and 12 weeks after ovariectomy (Fig. 1a-d). In order to compare the effect of bilateral ovariectomy on the aged rat model, 12-months old, non-ovariectomized SD rats served as old, healthy (OH) controls (Fig. 1e-h). *In vivo* μ CT imaging revealed a dense trabecular structure up to 4 weeks after the ovariectomy timepoint for the Osteo and the OH control group (Fig. 1a-b, e-f). However, the trabecular bone structure decreased already after 8 weeks (Fig. 1c, blue arrow) and even more pronounced after 12 weeks in the Osteo group (Fig. 1d, blue arrow), especially when compared with the OH group (Fig. 1h, yellow arrow). Age-related reduction of trabecular bone was also observable in the OH group when compared to the JH group (data not shown). In order to evaluate whether ovariectomy negatively affects the female SD rats, the animals were regularly monitored and their bodyweight recorded at all *in vivo* μ CT time points. After ovariectomy, visual monitoring by caretakers and researchers revealed no adverse effects on the rats' drinking and eating behavior. Moreover, the bodyweight records showed no significant differences between the Osteo and OH groups during the 12 weeks of osteoporosis progression (Fig. 1i).

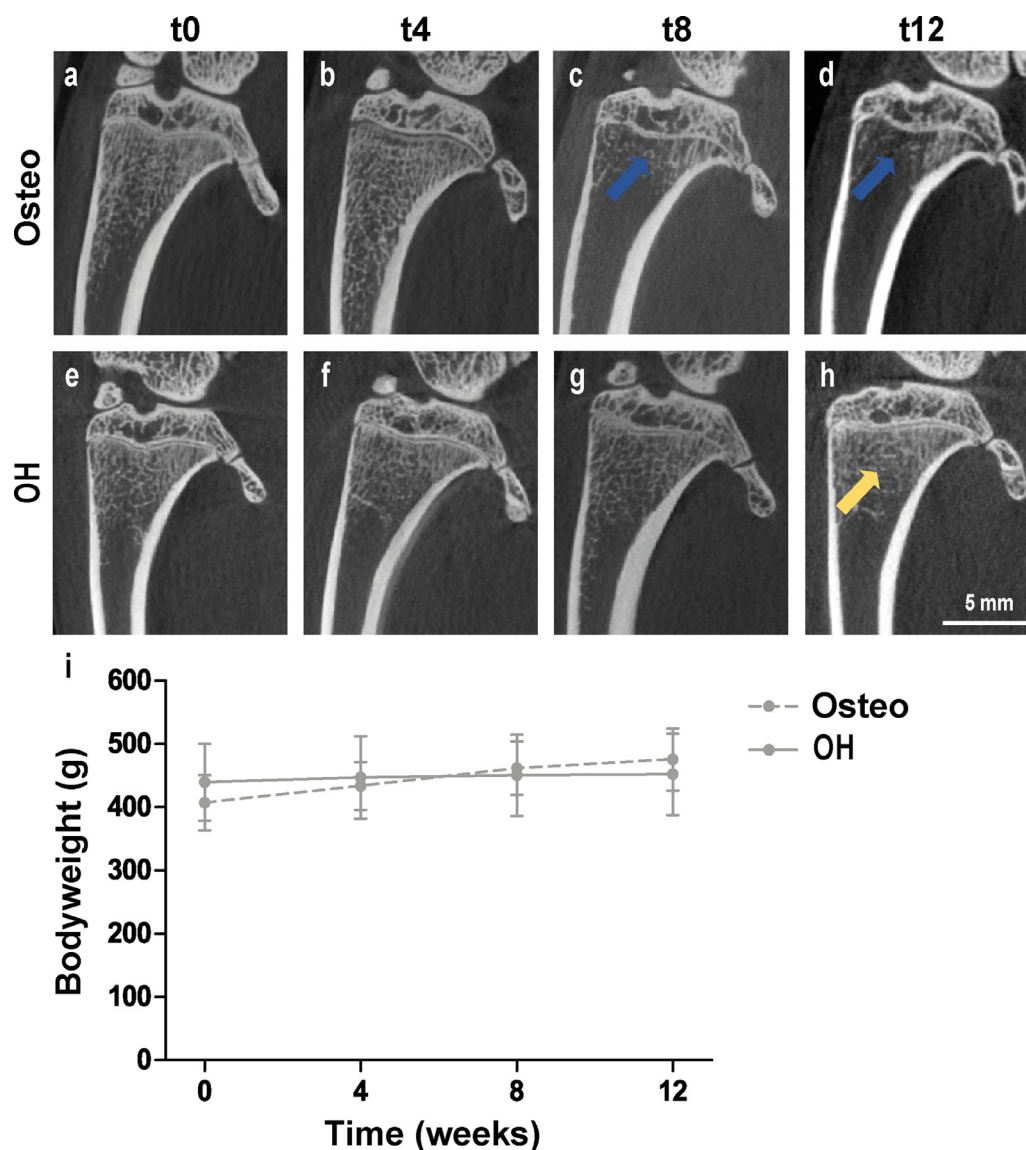


Fig. 1. Representative image of ovariectomy-induced osteoporosis progression. (a-d) Ovariectomy-induced osteoporosis progression over 12 weeks for SD rats that underwent bilateral ovariectomy at the age of 12 months (Osteo group). μ CT scans were performed (a) before ovariectomy, and (b) 4 weeks, (c) 8 weeks and (d) 12 weeks after ovariectomy. (e-h) μ CT scans of healthy rats with the same starting age of 12 months without ovariectomy (OH control group) measured over a period of 12 weeks. (i) Monitoring of bodyweight over the observation period. The blue and yellow arrows indicate a decreased trabecular bone structure in the Osteo group (c,d), compared to the OH group (h).

3.2. In vivo μ CT scans in osteoporotic, old healthy and juvenile healthy rats

Twelve weeks after ovariectomy, the Osteo and OH rats underwent bilateral, transcortical implantation of ZX00 pins into the proximal metaphysis of the tibiae, while the JH rats underwent the same ZX00 implantation at 6 weeks of age. The bodyweight of all three groups was continuously measured to observe any potential adverse effect from the surgical procedure or the ZX00 material (Supplementary Fig. S1). In the aged groups we observed a slight decrease in bodyweight within the first three weeks after ZX00 implantation, which leveled out until 24 weeks of implantation time (Supplementary Fig. S1a and b). As expected, the JH rats significantly gained weight until the end of the study (Supplementary Fig. S1c).

As illustrated in Fig. 2, the μ CT scans revealed radiolucent zones, which were more pronounced around the ZX00 implants in the tibiae of the aged rats compared to the JH rats, indicating increased gas volume in the aged rats. In detail, large radiolucent zones and new-bone formation (blue arrows) were observed in the

Osteo group already after 2 weeks post-implantation (Fig. 2b), and sclerotic rims developed after 6 weeks in three out of the seven osteoporotic rats (yellow arrows in Fig. 2c-f). The sclerotic rims, as a sign of foreign-body reaction, were observed in at least one or in both legs when the radiolucent zone around the implants was well pronounced. The OH rats (Fig. 2g-l) showed larger radiolucent zones than the JH rats (Fig. 2m-r), but when compared to the Osteo rats the radiolucent zones were smaller and sclerotic rims were not observed. As expected, gas volume was hardly detectable in the JH rats, and movement of the ZX00 implants away from the joint was seen due to the longitudinal bone growth of the juvenile rats.

3.3. Implant volume and surface area

To quantify the differences in implant degradation between the Osteo, OH and JH groups, μ CT images were three-dimensionally reconstructed and implant volume and surface area calculated with MIMICS software. At the beginning of the study, the average ZX00 implant volume was $15.88 \pm 0.68 \text{ mm}^3$. In all three groups, the implant volume monotonously degraded over 24 weeks (Fig. 3A).

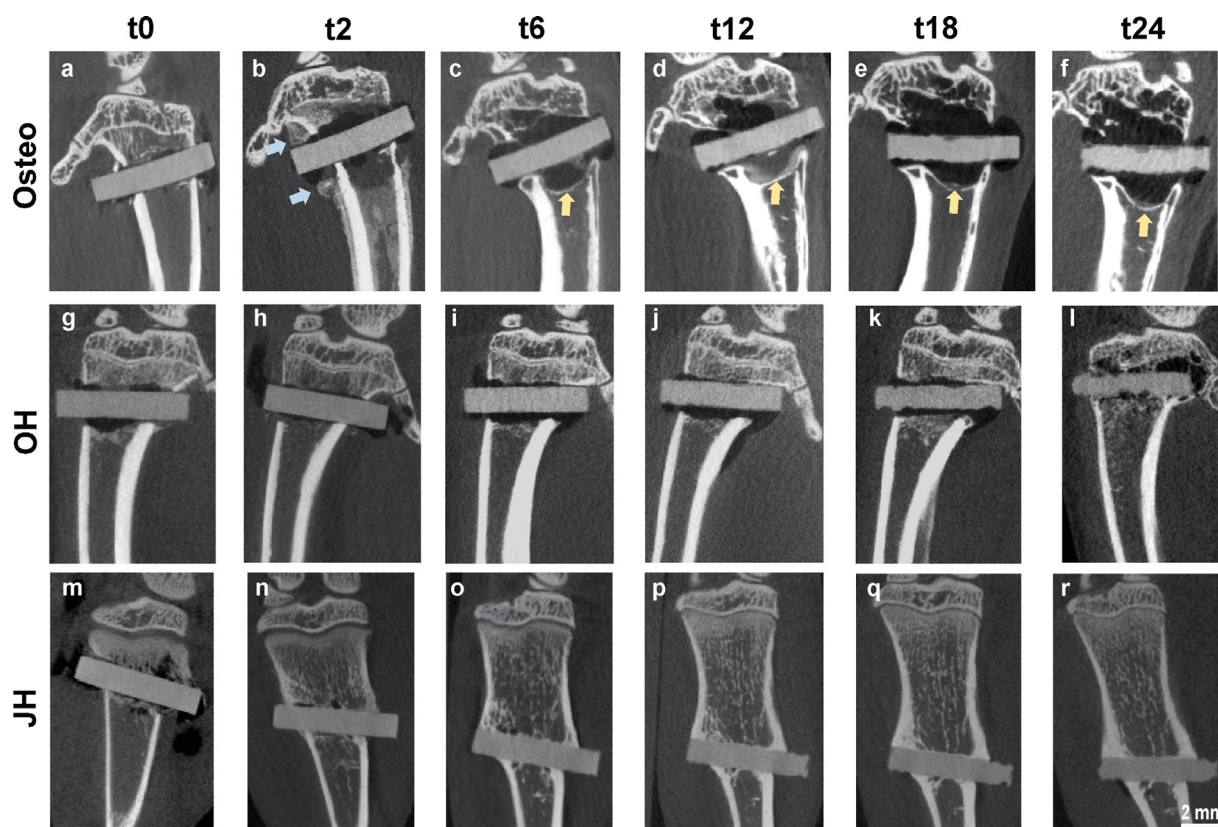


Fig. 2. ZX00 implant degradation over 24 weeks. Upper row: Osteo group that received implants 12 weeks after ovariectomy, i.e. at an age of 15 months. μ CT scans were performed (a) immediately and (b-f) 4–24 weeks after implantation. Middle row: OH control group without ovariectomy (g-l), which received implants at an age of 15 months. Lower row: JH control group (m-r), which received implants at an age of 6 weeks. The arrows in the Osteo group point to large radiolucent zones and new-bone formation 2 weeks after surgery (blue arrows) and sclerotic rims that developed 6 weeks post-operatively (yellow arrows).

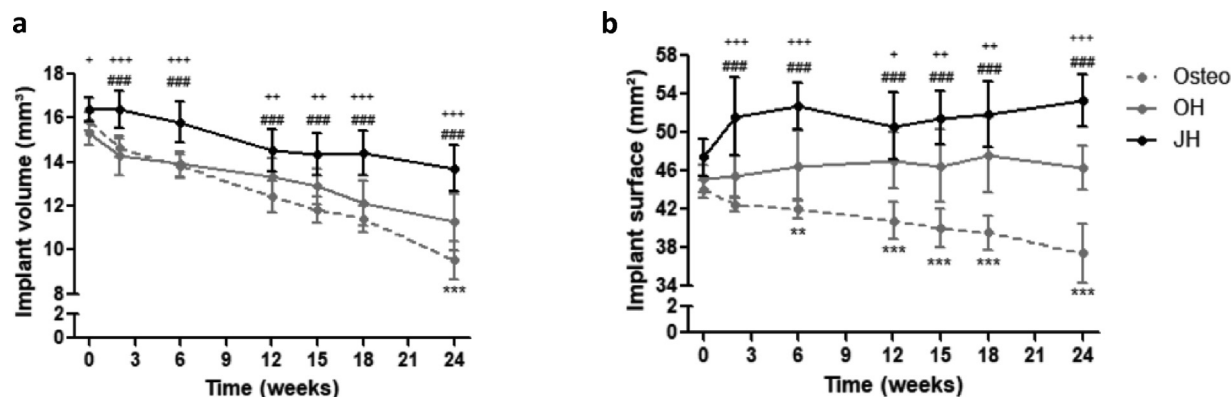


Fig. 3. Implant volume and surface over 24 weeks. (a) Implant volume and (b) implant surface obtained from three-dimensional reconstructions of the μ CT images evaluated using MIMICS software. Data is expressed as mean \pm standard deviation. A p-value of < 0.05 was considered as statistically significant. * $p < 0.05$, ** $p < 0.01$, *** $p < 0.001$ (same for the other marks # and +). #: Significant difference between Osteo and JH; #: significant difference between Osteo and JH; +: significant difference between OH and JH.

However, the implant volume loss was more pronounced in the aged groups (Osteo: grey dashed line, OH: grey solid line) compared to the JH rats (black line). In detail, the aged groups revealed significantly decreased implant volume already at 2 weeks post-implantation and this trend continued until the end of the study when compared to the JH group. Although there was no significant difference between the aged groups in the beginning of the study, we observed larger implant degradation in the Osteo group at 12 weeks, which culminated in a significantly reduced implant volume in the Osteo group compared to the OH

group 24 weeks after implantation. In total the implant volume loss of $40.89 \pm 3.53\%$ in the Osteo group was significantly higher than in the OH group ($24.21 \pm 5.42\%$, $p = 0.0016$) and JH group ($17.27 \pm 1.94\%$, $p = 0.0002$) over the entire study duration of 24 weeks.

We also observed major differences in the progress of implant surface area, especially between the Osteo and healthy groups (Fig. 3B). While the Osteo group revealed a monotonous decrease in implant surface area, the surface area in the healthy groups even increased in a slightly wavy pattern. In general, it decreased sig-

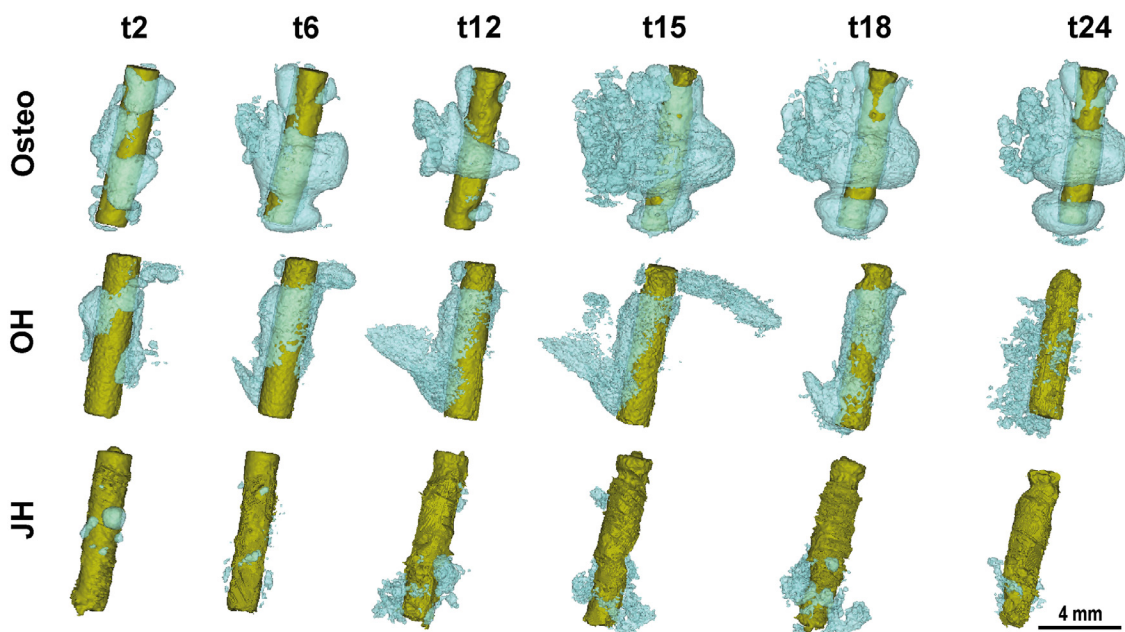


Fig. 4. 3D reconstructed ZX00 implant and surrounding gas volume. Upper row: Three-dimensional reconstructions of the μ CT images for the Osteo group 2–24 weeks after implantation, showing the ZX00 implants (ocher yellow) and released gas (cyan), Middle row: OH control group without ovariectomy. Lower row: JH control group.

nificantly in the Osteo group after 6 weeks compared to the OH group and already after 2 weeks compared to the JH group, and this trend continued until the end of the study. Moreover, after 2 weeks the implant surface area was reduced significantly in the OH group compared to the JH group, which also remained until the study end.

3.4. Gas volume

The three-dimensional reconstructions of the μ CT images revealed for the osteoporotic rats an increase in gas formation (cyan) around the ZX00 implants (ocher yellow) over the entire study period of 24 weeks (Fig. 4, upper panel). Moreover, the gas volume appears significantly more pronounced in the Osteo rats than in the OH rats (Fig. 4, upper and middle panel), which by itself was significantly more pronounced than in the JH rats (Fig. 4, lower panel).

In order to confirm this observation, we computed the gas volume for all three groups (Fig. 5). We observed a moderate gas evolution in the JH rats over the entire study duration (Fig. 5, black line), while gas volume was significantly increased 6 weeks after implantation in the Osteo group (grey dashed line) compared to the OH group (grey solid line) and JH group. The calculation of gas volume in the Osteo rats revealed a significant increase in gas volume already 2 weeks after implantation until 18 weeks post-implantation when compared to the JH group, but we did not observe any statistically significant differences in gas volume among the healthy groups. Taken together the results reveal the highest gas volume in the osteoporotic animals between 6 and 15 weeks after implantation, which on average, however, did not exceed 28 mm^3 .

3.5. Degradation rate

To compute an average degradation rate, we chose the average values of implant volume and surface area at time points 0 and 24 weeks. As expected from the previous results, the average degradation rates up to 24 weeks after implantation were highest in

the Osteo group ($0.35 \pm 0.06 \text{ mm/year}$), followed by the OH group ($0.18 \pm 0.07 \text{ mm/year}$) and the JH group ($0.12 \pm 0.04 \text{ mm/year}$). Taken together, the degradation rate in osteoporotic rats was almost twice as high as in the OH group and almost three times higher than in the JH group.

3.6. High-resolution SR μ CT imaging

Fig. 6 shows SR μ CT images that reveal the degradation of the ZX00 pins and in-grown bone at high resolution. Both the residual metal and the degradation layer that has formed during the degradation process are visible. Some cracks are present within the degradation layer, which may be caused by the drying and/or embedding process. The bone is well visible along with vascular channels and lacunae, and also the epiphyseal line can be well distinguished within the bone. A bone layer that has formed around the implant can be observed in all three groups. However, the pin in the Osteo group has degraded more significantly and is surrounded by a thinner bone layer and less amount of bone overall. The same holds true for all eight samples that were assessed in this study (see Supplementary Fig. 2). These qualitative observations were quantified in Avizo, as described in section 2.6, to obtain the bone-volume content f_{bone} (Fig. 6g). It is lowest for the Osteo group, higher for the OH group, and highest for the JH group. The mean trabecular thickness calculated for the Osteo group was $113.5 \pm 2.0 \mu\text{m}$, which was slightly lower compared to $115.1 \pm 0.7 \mu\text{m}$ for the OH group. Similarly, the mean connectivity Conn.D was lower for the Osteo group than for the OH group, with $44.8 \pm 25.0 \text{ mm}^{-3}$ and $121.1 \pm 35.4 \text{ mm}^{-3}$, respectively.

3.7. Qualitative histology

The histological evaluation revealed a homogeneous and occasionally lacuna-shaped degradation (pit corrosion) of the ZX00 pins (Fig. 7). For all groups the pins are still preserved to a large extent over the entire study period of 24 weeks. The metallic regions are surrounded with corrosion products, reaching a layer thickness of approximately $150 \mu\text{m}$. Since the corrosion products largely contain

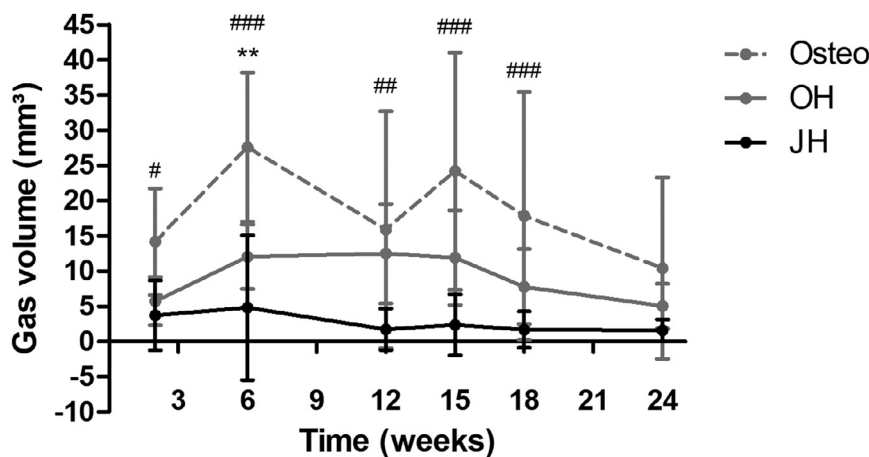


Fig. 5. Reconstructed gas volume. Reconstructed gas volume calculated from the 3D reconstructions of the μ CT images over the study period of 24 weeks for the Osteo group (grey dashed line), OH group (grey solid line), and JH group (black solid line). Data is expressed as mean \pm standard deviation. A p-value of < 0.05 was considered as statistically significant. * $p < 0.05$, ** $p < 0.01$, *** $p < 0.001$ (same for the mark #). *: Significant difference between Osteo and OH; #: significant difference between Osteo and JH. No significant difference was observed between the healthy groups (OH and JH).

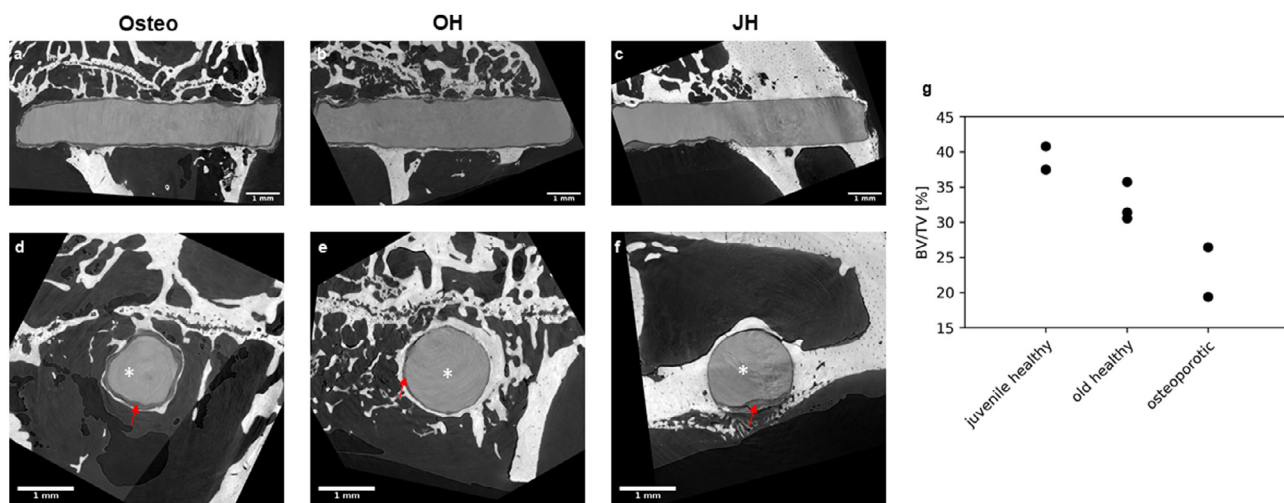


Fig. 6. Tomographic reconstruction of SR μ CT images and calculated BV/TV. (a–f) 3D tomographic reconstruction of samples imaged via SR μ CT after 24 weeks of implantation. Upper row: Slices along the pin’s longitudinal axis. Lower row: Slices along the cross-section of the pin. (g) Bone-volume fraction (f_{bone}) as calculated from the region of interest around the pin ($\varnothing = 1.6$ mm), having a diameter enlarged by 1 mm. Three samples were imaged each for the JH and OH groups and two for the Osteo group (see also Supplementary Fig. S2). The degradation layer (red arrow) and the residual metal (white star) of the pins are well visible, together with the surrounding bone.

Ca and P [55], which is also largely contained in bone, the staining of these regions appears similar to bone (in pink). The degradation layer may be distinguished from bone by the shade, morphology and the existence of osteocytes [55,56]. The ZX00 pins are surrounded by gas cavities that take less area in the JH and OH groups (Fig. 7b and c), compared to the Osteo group (Fig. 7a). In all samples, no fibrous capsules were observed.

4. Discussion

The advancing prevalence of osteoporosis is associated with increasing age of the population. The World Health Organization predicts a doubling of the number of people aged over 60 and a tripling of those older than 80 by 2050 [57]. Osteoporosis is characterized by decreased peak bone mass and density, decreased mineralization and increased risk of fragility fractures. Senile osteoporosis predominantly occurs in elderly people starting in their 70s [58], whereas one out of two women suffer from postmenopausal osteoporosis linked to estrogen-deficiency [59]. The

strong increase in age and the associated chance to suffer from one or even several new fractures at an advanced age presents a new challenge to orthopedic surgeons.

Here, we propose that low-alloyed Mg-based ZX00 implants might overcome the disadvantages associated with permanent implants and, because of ZX00’s low degradation rate, may fulfill the mechanical properties needed to stabilize osteoporotic fractures. Upon degradation, ZX00 also releases Mg^{2+} ions that might be beneficial to support bone formation.

Cylindrical ZX00 pins were transcortically implanted into the proximal metaphysis of the tibiae in ovariectomy-induced osteoporotic (Osteo), old healthy (OH) and juvenile healthy (JH) Sprague Dawley rats. Bilateral ovariectomy was performed in 12-months old rats to induce osteoporosis, and osteoporosis progression was observed by *in vivo* μ CT. We demonstrate that ovariectomy results in reduced trabecular bone already after 8 weeks, and that this effect is even more pronounced after 12 weeks. This result is in accordance with other studies using an ovariectomy-induced osteoporotic rat model [60,61]. Here, several studies on osteoporotic

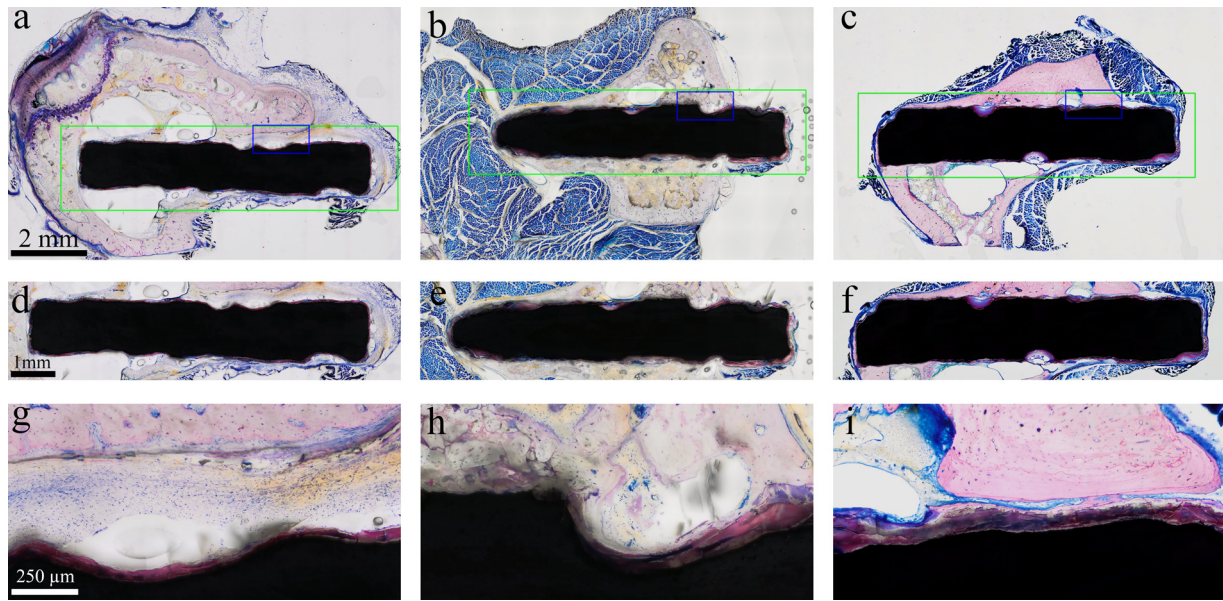


Fig. 7. Histological investigation. Undecalcified thin ground sections of samples after 24 weeks of implantation stained with Laczo, Levai. The dyes stain soft tissue blue and calcified tissue in shades of pink, with older bone appearing lighter than younger bone. First column (a, d, g) show the Osteo, second column (b, e, h) the OH and third column (c, f, i) the JH group. First row shows overviews of the thin ground sections of horizontal cuts through the tibia. Green, larger and blue smaller rectangles are locations of the magnification in second and third row respectively. The second row shows the area of and surrounding the pins. Degradation is visible on the surface of the implant as a perimeter in pink. In (d) only bone to degradation area contact in the inserted end is observable, bone is separated from implant in the cortical region. In (g) detail of the implant separation between implant and bone by soft tissue; cell less, pink degradation area is visible. In (e) bone surrounds the implant and is in contact with the degradation area, only a few locations in the bone and the right tip of the implant is bone contact free. In (h) the detail of the implant bone is in contact with the degradation area on the left side newly formed bone connects old bone sequesters and is in contact the undegraded part of the implant. New bone was added to a resorbed surface in the middle of the image bone is newly formed. In (f) bone surrounds the implant to a large amount, and mostly in contact with the degradation area, only at the right tip of the implant bone is in contact to the undegraded implant. In (i) the detail of the implant a thin newly formed bone layer is in contact with the thick degradation area and only in contact with the old bone via a small bridge, soft tissue separates the newly formed and old bone in the most parts.

animals used female rats that underwent ovariectomy at the age of 3–6 months [62,63]. Below 6 months of age, however, the ovariectomy-induced osteoporosis model shows some major disadvantages and therefore limits the validity of the results [64,65]. For instance, in 3-months old ovariectomy-induced osteoporotic rats longitudinal bone growth still occurs and, accordingly, connectivity of trabeculae is increased compared to old rats [66]. Since rats are known to reach skeletal maturation at the age of 6–10 months and senile osteoporosis mainly occurs after one year, we thus chose the presented aged model to induce estrogen deficiency *via* ovariectomy making it more comparable to the human situation. In this way, we observed an age- and estrogen-deficiency-related reduction of trabecular bone also in the OH control group, which indicates bone loss over time and might be associated with progressing ovariectomy-induced osteoporosis, as also proposed in other studies [67].

Bilateral, transcortical implantation of ZX00 pins was performed on rats at the ages of 15 months (Osteo and OH group) and 6 weeks (JH group), and *in vivo* μ CT imaging was done at several time points after surgery (Fig. 2). Reconstruction of these μ CT data revealed a significantly decreased implant volume in the Osteo and OH rats compared to the JH rats for the entire study duration, and a significantly reduced implant volume of the Osteo rats compared to the OH rats after 24 weeks of surgery (Fig. 3a). Moreover, the implant surface of the Osteo rats was found to be significantly decreased compared to the healthy rats (OH and JH group) for the entire study period (Fig. 3b). Combining the computations for implant volume and surface, we conclude that the degradation rate is highest in ovariectomy-induced osteoporotic rats followed by old and juvenile healthy rats. A previous study performed by the authors showed promising results in terms of the degradation of ZX00 implanted into the diaphysis of juvenile rat femurs, where ZX00 was found to degrade monotonously with a volume

loss of 19% after 24 weeks of implantation, suggesting a total resorption after two years [34]. Other researchers suggested that implant degradation may be affected by the implantation site since bone repair in the metaphysis depends on bone marrow stromal cells, whereas periosteum plays a key role in diaphyseal bone repair [68]. However, in the present study, computing the volume loss of ZX00 implants in the proximal metaphysis of the tibiae revealed a degradation of $17.27 \pm 1.94\%$ over 24 weeks, which indicates a comparable degradation rate independent of the implantation site.

The usage of Mg as an implant material that releases Mg ions for the beneficial support of bone formation is not a new idea [69,70], but studies in old and, especially, in osteoporotic animals are rare. In literature, there are only few studies that investigated Mg-based implants or Mg-coating on Ti alloys in osteoporotic bone. One study [71] evaluated the beneficial effect of immersing Ti mini-screws in magnesium-chloride solution before implanting them into the tibiae and femurs of ovariectomy-induced osteoporotic rats. Seven days after implantation, significantly increased new-bone volume was observed in the group with magnesium-immersed Ti mini-screws compared to the untreated Ti screws. Zhang et al. [37] further demonstrated Mg's role in the bone-fracture repair of osteoporotic rats by promoting CGRP-mediated differentiation of osteogenic effects. Previously, the combination of Mg and zoledronic acid has been demonstrated to have beneficial effects on osteogenesis and inhibitory effects on osteoclastogenesis [66]. Bilayer coating on a Mg–Nd–Zn–Zr (JDBM) alloy resulted in controlled Mg degradation and improved osseointegration. By incorporation of zoledronic acid (ZA) into the coating, intramedullary nails based on the JDBM alloy (designated as Mg/Zn/CaP) revealed the greatest callus formation and accelerated bone formation after 12 weeks. Additionally, mechanical performance was improved in the Mg/Zn/CaP group after 12 weeks. The researchers concluded

that the co-delivery strategy improved the treatment efficacy in osteoporotic bone [72]. However, the study duration of these few projects was short and, to the best of our knowledge, this present study is the first that reports Mg-implant degradation for a study duration of 24 weeks in ovariectomy-induced osteoporotic rats.

Unpredictable degradation behavior and related major hydrogen gas formation have long limited Mg's application in orthopedic surgery. Several studies have been conducted, investigating various Mg-based alloys of different composition, with and without surface modification, in order to achieve more information on degradation behavior, osseointegration, gas formation, accumulation of degradation products, impact on juvenile bone growth, and general tolerance, i.e. induction of systemic inflammatory reactions [34,55,73–78]. Most of the studies used Mg alloys with the addition of rare-earth elements, with some of them known to slow down Mg's degradation rate. However, ZX00 is a Mg–Zn–Ca alloy with an exceptionally low amount of alloying elements, which is solely based on materials that occur naturally in the human body and therefore may also be safely applied in patient cohorts such as children. In the present study, we demonstrate that ZX00 monotonously degrades and only generates moderate gas evolution in juvenile healthy (JH) rats. In contrast, the gas volume was significantly increased in ovariectomy-induced osteoporotic (Osteo) rats compared to the JH rats already after 2 weeks, and this trend continued until the end of the study. Two weeks after implantation, the gas volume was also increased in the Osteo rats compared to the old healthy (OH) rats. Additionally, bone in-growth and osseointegration was not observable in the Osteo rats. These results indicate that the underlying reason for increased degradation rates and, accordingly, increased gas formation can be attributed to the bone condition.

We also observed sclerotic rim formation in three out of seven osteoporotic rats, at least in one or even both legs. Sclerotic rims have been described to develop in order to protect the bone-marrow cavity from foreign bodies [79]. Since sclerotic rims were only observed when gas volume strongly increased, we assume that the bone perceives a rapidly degrading implant as a foreign body and immediately responds by developing a sclerotic rim to protect the bone-marrow cavity and the bone-marrow stromal cells. In clinics, sclerotic rims develop to prevent or delay the bone from osteonecrotic collapse by providing mechanical support [80]. Osteoporosis is associated with a low-grade inflammatory state tagged by increased cytokines, such as TNF α and IL-1 β . Inflammation may induce a pH drop leading to acidosis. However, little is known about the influence of the local bone environment on Mg degradation [81]. High pH values over 11.5 promote a stable hydroxide layer on Mg's surface, while pH values below 11.5 support implant degradation. Accordingly, an increased Mg-implant degradation rate is suggested *in vivo* due to a physiological pH value of 7.4.

In general, since we aimed to evaluate the *in vivo* response to ovariectomy, the μ CT scans had to be performed at relatively low resolution, so that a quantification of the bone-mineral density was impossible. Nevertheless, osteoporosis progression was still conclusive and an obvious decrease of the trabecular structure was observed. Moreover, the bone-volume fraction, as quantified by high-resolution SR μ CT (see Fig. 6), was found to be reduced in the Osteo group compared to the OH and JH groups. This is in line with other findings on the impact of osteoporosis on bone-volume fraction [82–84]. Similarly, in line with previous studies we found that the trabecular thickness was similar for the Osteo group and for the OH group, while the connectivity was reduced [85]. The mean values agree well with those observed in the literature, suggesting that the implants' presence had no significant influence on the trabecular bone volume. Qualitative histological analysis confirmed the increased gas formation under osteoporotic conditions, follow-

ing the enhanced implant degradation in the Osteo group. The increased gas formation could be the reason for less bone integration, with a large amount of soft tissue in contact with the degradation area. The degradation seems to be in an advanced state in which the implant appears homogeneously degraded with less deep pit corrosions compared to the other groups. OH and JH group showed better bone integration and less overall degradation, however, locally deeper pit corrosions.

5. Summary and conclusions

In summary, we demonstrate increased ZX00 implant degradation in ovariectomy-induced osteoporotic (Osteo) rats compared to old healthy (OH) and juvenile healthy (JH) animals. Sclerotic rim development was observed in about half of the Osteo rats, suggesting that bone prevents itself from the (rapidly degrading) foreign body and from osteonecrosis development. Osteoporosis-associated low-grade inflammation may decrease the pH value, resulting in accelerated ZX00 implant degradation with increased gas formation. However, further studies are needed to unravel the underlying metabolic and biochemical mechanisms behind this phenomenon. Furthermore, it still remains unclear whether osteoporotic bone increases ZX00 degradation to compensate for its Ca/Mg deficiency. Therefore, studies may be needed that focus on the application of Mg-based implants in estrogen- and/or Ca/Mg-supplemented osteoporotic models to investigate whether Mg-implant degradation will be decreased because the compensation for Ca/Mg deficiency would then become unnecessary. To date, ZX00 provides a promising implant material for young and older healthy patients. This study suggests, however, that ZX00 may not be of advantage in untreated osteoporotic conditions, and it can be safely assumed that this also applies to other Mg-based implants, including those containing rare-earth elements.

Declaration of Competing Interest

We declare that the Medical University of Graz received funding from the "Österreichische Gesellschaft für Knochen- und Mineralstoffwechsel" (ÖGKM). Prof. Annelie-Martina Weinberg is a shareholder and consultant of Bioretec Ltd.

Acknowledgements

We thank Dr. Vladimir Bubalo and his team as well as the pre-clinical imaging team at the Biomedical Research Facility, Medical University of Graz for technical support with the ovariectomy and imaging. This work was supported by the ÖGKM, Swiss National Science Foundation (SNF Sinergia, Grant No. CRSII5-180367) and the Laura Bassi Center of Expertise BRIC (Bioresorbable Implants for Children, FFG –Austria). HC and BO acknowledge funding from the European Union's Horizon 2020 research and innovation program under the Marie Skłodowska-Curie grant, agreement No 811226. We thank the Diamond Light Source for granting beamtimes MG25485-3 and MG25485-4 at the beamline I13-2, and thank Christian Rau and Shashidhara Marathe for support during the measurements.

Supplementary materials

Supplementary material associated with this article can be found, in the online version, at doi:10.1016/j.actbio.2022.05.041.

References

- [1] E. Curtis, R. Moon, N. Harvey, C. Cooper, Reprint of: The impact of fragility fracture and approaches to osteoporosis risk assessment worldwide, *International Journal of Orthopaedic and Trauma Nursing* 26 (2017) 7–17.

- [2] R. Pivonello, A.M. Isidori, M.C. De Martino, J. Newell-Price, B.M. Biller, A. Colao, Complications of Cushing's syndrome: state of the art, *The Lancet* 4 (2016) 611–629, doi:10.1016/S2213-8587(16)00086-3.
- [3] N.E. Lane, etiology Epidemiology, diagnosis of osteoporosis, *American Journal of Obstetrics and Gynecology* 194 (2006) 3–11, doi:10.1016/j.ajog.2005.08.047.
- [4] R. Nuti, M. Brandi, G. Checchia, O. Di Munno, L. Dominguez, P. Falaschi, C. Fiore, G. Iolascon, S. Maggi, R. Michieli, Guidelines for the management of osteoporosis and fragility fractures, *Internal and Emergency Medicine* 14 (2019) 85–102, doi:10.1007/s11739-018-1874-2.
- [5] M.-X. Ji, Q. Yu, Primary osteoporosis in postmenopausal women, *Chronic Dis Transl Med* 1 (2015) 9–13, doi:10.1016/j.cdtm.2015.02.006.
- [6] M. Haffner-Luntzer, V. Fischer, K. Prystaz, A. Liedert, A. Ignatius, The inflammatory phase of fracture healing is influenced by oestrogen status in mice, *Eur J Med Res* 22 (2017) 1–11, doi:10.1186/s40001-017-0264-y.
- [7] K. Li, X.-F. Wang, D.-Y. Li, Y.-C. Chen, L.-J. Zhao, X.-G. Liu, Y.-F. Guo, J. Shen, X. Lin, J. Deng, R. Zhou, H.-W. Deng, The good, the bad, and the ugly of calcium supplementation: a review of calcium intake on human health, *Clin Interv Aging* 13 (2018) 2443–2452, doi:10.2147/CIA.S157523.
- [8] M. Mizokuchi, M. Kubota, Y. Tomino, H. Koide, Possible mechanism of impaired calcium and vitamin D metabolism in nephrotic rats, *Kidney International* 42 (1992) 335–340, doi:10.1038/ki.1992.294.
- [9] J. Fong, A. Khan, Hypocalcemia: Updates in diagnosis and management for primary care, *Canadian Family Physician* 58 (2012) 158–162.
- [10] J. Zhao, A. Giri, X. Zhu, M.J. Shrubsole, Y. Jiang, X. Guo, R. Ness, D.L. Seidner, E. Giovannucci, T.L. Edwards, Q. Dai, Calcium: magnesium intake ratio and colorectal carcinogenesis, results from the prostate, lung, colorectal, and ovarian cancer screening trial, *Br J Cancer* 121 (2019) 796–804, doi:10.1038/s41416-019-0579-2.
- [11] E.A. Hibler, X. Zhu, M.J. Shrubsole, L. Hou, Q. Dai, Physical activity, dietary calcium to magnesium intake and mortality in the National Health and Examination Survey 1999–2006 cohort, *International Journal of Cancer* 146 (2020) 2979–2986, doi:10.1002/ijc.32634.
- [12] D.A. Straub, Calcium Supplementation in Clinical Practice: A Review of Forms, Doses, and Indications, *Nutrition in Clinical Practice* 22 (2007) 286–296, doi:10.1177/0115426507022003286.
- [13] L.T. Radford, M.J. Bolland, B. Mason, A. Horne, G.D. Gamble, A. Grey, I.R. Reid, The Auckland calcium study: 5-year post-trial follow-up, *Osteoporos Int* 25 (2014) 297–304, doi:10.1007/s00198-013-2526-z.
- [14] M. Ordak, M. Maj-Zurawska, H. Matsumoto, M. Bujalska-Zadrozny, I. Kieres-Salomonski, T. Nasierowski, E. Muszynska, M. Wojnar, Ionized magnesium in plasma and erythrocytes for the assessment of low magnesium status in alcohol dependent patients, *Drug and Alcohol Dependence* 178 (2017) 271–276, doi:10.1016/j.drugalcdep.2017.04.035.
- [15] M. Barbagallo, N. Veronese, L.J. Dominguez, Magnesium in Aging, *Health and Diseases*, *Nutrients* 13 (2021) 463, doi:10.3390/nu13020463.
- [16] M.M. Belluci, G. Giro, R.A.L. del Barrio, R.M.R. Pereira, E. Marcantonio, S.R.P. Orrico, Effects of magnesium intake deficiency on bone metabolism and bone tissue around osseointegrated implants, *Clinical Oral Implants Research* 22 (2011) 716–721, doi:10.1111/j.1600-0501.2010.02046.x.
- [17] A.L. Boskey, C.M. Rinnac, M. Bansal, M. Federman, J. Lian, B.D. Boyan, Effect of short-term hypomagnesemia on the chemical and mechanical properties of rat bone, *Journal of Orthopaedic Research* 10 (1992) 774–783, doi:10.1002/jor.1100100605.
- [18] A.L. Tranquilli, E. Lucino, G.G. Garzetti, C. Romanini, Calcium, phosphorus and magnesium intakes correlate with bone mineral content in postmenopausal women, *Gynecological Endocrinology* 8 (2009) 55–58, doi:10.3109/09513599409028459.
- [19] R.K. Rude, F.R. Singer, H.E. Gruber, Skeletal and Hormonal Effects of Magnesium Deficiency, *Journal of the American College of Nutrition* 28 (2009) 131–141, doi:10.1080/07315724.2009.10719764.
- [20] H.Y. Kim, J.W. Choe, H.K. Kim, S.J. Bae, B.J. Kim, S.H. Lee, J.-M. Koh, K.O. Han, H.M. Park, G.S. Kim, Negative Association between Metabolic Syndrome and Bone Mineral Density in Koreans, Especially in Men, *Calcified Tissue International* 86 (2010) 350–358, doi:10.1007/s00223-010-9347-2.
- [21] R.D. Bukoski, Reactive oxygen species: the missing link between magnesium deficiency and hypertension, *J Hypertens* 20 (2002) 2141–2143, doi:10.1097/00004872-200211000-00009.
- [22] M.G. Huerta, J.N. Roemmich, M.L. Kington, V.E. Bovbjerg, A.L. Weltman, V.F. Holmes, J.T. Patrie, A.D. Rogol, J.L. Nadler, Magnesium Deficiency Is Associated With Insulin Resistance in Obese Children, *Diabetes Care* 28 (2005) 1175–1181, doi:10.2337/diacare.28.5.1175.
- [23] S. Manolagas, R. Jilka, Bone Marrow, Cytokines, and Bone Remodeling – Emerging Insights into the Pathophysiology of Osteoporosis, *The New England Journal of Medicine* (1995) 305–311, doi:10.1056/NEJM199502023320506.
- [24] S. Larsson, Treatment of Osteoporotic Fractures, *Scand J Surg* 91 (2002) 140–146, doi:10.1177/145749690209100202.
- [25] V. Alt, U. Thormann, S. Ray, D. Zahner, L. Dürselen, K. Lips, T. El Khassawna, C. Heiss, A. Riedrich, G. Schlewitz, A. Ignatius, M. Kampschulte, H. von Dewitz, S. Heinemann, R. Schnettler, A. Langheinrich, A new metaphyseal bone defect model in osteoporotic rats to study biomaterials for the enhancement of bone healing in osteoporotic fractures, *Acta Biomaterialia* 9 (2013) 7035–7042, doi:10.1016/j.actbio.2013.02.002.
- [26] M. Kherad, D. Mellström, B.E. Rosengren, R. Hasserijs, J.-Å. Nilsson, I. Redlund-Johnell, C. Ohlsson, M. Lorentzon, M.K. Karlsson, The number and characteristics of prevalent vertebral fractures in elderly men are associated with low bone mass and osteoporosis, *The Bone & Joint Journal*. 97-B (2015) 1106–1110, doi:10.1302/0301-620X.97B8.35032.
- [27] N. Mathavan, M. Tägil, H. Isaksson, Do osteoporotic fractures constitute a greater recalcitrant challenge for skeletal regeneration? Investigating the efficacy of BMP-7 and zoledronate treatment of diaphyseal fractures in an open fracture osteoporotic rat model, *Osteoporos Int* 28 (2017) 697–707, doi:10.1007/s00198-016-3771-8.
- [28] L. Chen, L. Yang, M. Yao, X.-J. Cui, C.-C. Xue, Y.-J. Wang, B. Shu, Biomechanical Characteristics of Osteoporotic Fracture Healing in Ovariectomized Rats: A Systematic Review, *PLOS ONE* 11 (2016) e0153120, doi:10.1371/journal.pone.0153120.
- [29] N. Mathavan, M. Tägil, H. Isaksson, Do osteoporotic fractures constitute a greater recalcitrant challenge for skeletal regeneration? Investigating the efficacy of BMP-7 and zoledronate treatment of diaphyseal fractures in an open fracture osteoporotic rat model, *Osteoporosis International* 28 (2016) 697–707, doi:10.1007/s00198-016-3771-8.
- [30] H. Zhang, C.G. Lewis, M.G. Aronow, G.A. Gronowicz, The effects of patient age on human osteoblasts' response to Ti–6Al–4V implants in vitro, *Journal of Orthopaedic Research* 22 (2004) 30–38, doi:10.1016/S0736-0266(03)00155-4.
- [31] P. Mendes Duarte, J.B.C. Neto, P.F. Gonçalves, E.A. Sallum, F.H. Nociti, Estrogen Deficiency Affects Bone Healing Around Titanium Implants: A Histometric Study in Rats, *Implant Dentistry* 12 (2003) 340–346, doi:10.1097/01.ID.0000099750.26582.4B.
- [32] N. Nicolini Aldini, M. Fini, G. Giavaresi, R. Giardino, T. Greggi, P. Parisini, Pedicular fixation in the osteoporotic spine: a pilot in vivo study on long-term ovariectomized sheep, *Journal of Orthopaedic Research* 20 (2002) 1217–1224, doi:10.1016/S0736-0266(02)00069-4.
- [33] C. Zhao, H. Wu, J. Ni, S. Zhan, X. Zhang, Development of PLA/Mg composite for orthopedic implant: Tunable degradation and enhanced mineralization, *Composites Science and Technology* 147 (2017) 8–15.
- [34] N.G. Grün, P. Holweg, S. Tangl, J. Eichler, L. Berger, J.J.P. van den Beucken, J.F. Löffler, T. Klestil, A.M. Weinberg, Comparison of a resorbable magnesium implant in small and large growing-animal models, *Acta Biomaterialia* 78 (2018) 378–386, doi:10.1016/j.actbio.2018.07.044.
- [35] P. Holweg, L. Berger, M. Cihova, N. Donohue, B. Clement, U. Schwarze, N. Sommer, G. Hohenberger, J.J.P. van den Beucken, F. Seibert, A. Leithner, J. Löffler, A.-M. Weinberg, A lean magnesium–zinc–calcium alloy ZX00 used for bone fracture stabilization in a large growing-animal model, *Acta Biomaterialia* 113 (2020) 646–659.
- [36] P. Holweg, V. Herber, M. Ornig, G. Hohenberger, N. Donohue, P. Puchwein, A. Leithner, F. Seibert, A lean bioabsorbable magnesium–zinc–calcium alloy ZX00 used for operative treatment of medial malleolus fractures, *Bone & Joint Research* 9 (2020) 477–483, doi:10.1302/2046-3758.98.BJR-2020-0017.R2.
- [37] Y. Zhang, J. Xu, Y.C. Ruan, M.K. Yu, M. O'Laughlin, H. Wise, D. Chen, L. Tian, D. Shi, J. Wang, S. Chen, J.Q. Feng, D.H.K. Chow, X. Xie, L. Zheng, L. Huang, S. Huang, K. Leung, N. Lu, L. Zhao, H. Li, D. Zhao, X. Guo, K. Chan, F. Witte, H.C. Chan, Y. Zheng, L. Qin, Implant-derived magnesium induces local neuronal production of CGRP to improve bone-fracture healing in rats, *Nat Med* 22 (2016) 1160–1169, doi:10.1038/nm.4162.
- [38] K. Jähn, H. Saito, H. Taipaleenmäki, A. Gasser, N. Hort, F. Feyerabend, H. Schlüter, J. Rueger, W. Lehmann, R. Willumeit-Römer, E. Hesse, Intramedullary Mg2Ag nails augment callus formation during fracture healing in mice, *Acta Biomaterialia* 36 (2016) 350–360.
- [39] Z. Zhai, X. Qu, H. Li, K. Yang, P. Wan, L. Tan, Z. Ouyang, X. Liu, B. Tian, F. Xiao, W. Wang, C. Jiang, Q. Fan, A. Qin, K. Dai, The effect of metallic magnesium degradation products on osteoclast-induced osteolysis and attenuation of NF- κ B and NFATc1 signaling, *Biomaterials* 35 (2014) 6299–6310.
- [40] J. Löffler, P. Uggowitzer, C. Wegmann, M. Becker, H. Feichtinger, Process and apparatus for vacuum distillation of high-purity magnesium, (2013).
- [41] C. Rau, U. Wagner, Z. Pešić, A. De Fanijs, Coherent imaging at the Diamond beamline I13, *Physica Status Solidi (a)* 208 (2011) 2522–2525, doi:10.1002/pssa.201184272.
- [42] Z.D. Pešić, A.D. Fanijs, U. Wagner, C. Rau, Experimental stations at I13 beamline at Diamond Light Source, *J. Phys.: Conf. Ser.* 425 (2013) 182003, doi:10.1088/1742-6596/425/18/182003.
- [43] B. Zeller-Plumhoff, D. Tolnai, M. Wolff, I. Greving, N. Hort, R. Willumeit-Römer, Utilizing Synchrotron Radiation for the Characterization of Biodegradable Magnesium Alloys—From Alloy Development to the Application as Implant Material, *Advanced Engineering Materials* 23 (2021) 2100197, doi:10.1002/adem.202100197.
- [44] A.D. Fanijs, Z.D. Pešić, U. Wagner, C. Rau, Fast X-ray imaging at beamline I13L at Diamond Light Source, *J. Phys.: Conf. Ser.* 425 (2013) 192014, doi:10.1088/1742-6596/425/19/192014.
- [45] N. Wadeson, M. Basham, Savu: A Python-based, MPI Framework for Simultaneous Processing of Multiple, N-dimensional, Large Tomography Datasets (2016) ArXiv:1610.08015 [Cs] <http://arxiv.org/abs/1610.08015>. (accessed December 14, 2021).
- [46] R.C. Atwood, A.J. Bodey, S.W.T. Price, M. Basham, M. Drakopoulos, A high-throughput system for high-quality tomographic reconstruction of large datasets at Diamond Light Source, *Philosophical Transactions of the Royal Society A: Mathematical, Physical and Engineering Sciences* 373 (2015) 20140398, doi:10.1098/rsta.2014.0398.
- [47] D. Gursoy, F. De Carlo, X. Xiao, C. Jacobsen, TomoPy: a framework for the analysis of synchrotron tomographic data, *J Synchrotron Radiat* 21 (2014) 1188–1193, doi:10.1107/S1600577514013939.

- [48] N.T. Vo, R.C. Atwood, M. Drakopoulos, Radial lens distortion correction with sub-pixel accuracy for X-ray micro-tomography, *Opt. Express*, OE. 23 (2015) 32859–32868, doi:[10.1364/OE.23.032859](https://doi.org/10.1364/OE.23.032859).
- [49] N.T. Vo, R.C. Atwood, M. Drakopoulos, Superior techniques for eliminating ring artifacts in X-ray micro-tomography, *Opt. Express*, OE. 26 (2018) 28396–28412, doi:[10.1364/OE.26.028396](https://doi.org/10.1364/OE.26.028396).
- [50] S. Bruns, S.L.S. Stipp, H.O. Sørensen, Looking for the Signal: A guide to iterative noise and artefact removal in X-ray tomographic reconstructions of porous geomaterials, *Advances in Water Resources* 105 (2017) 96–107, doi:[10.1016/j.advwatres.2017.04.020](https://doi.org/10.1016/j.advwatres.2017.04.020).
- [51] D. Krüger, S. Galli, B. Zeller-Plumhoff, D.C.F. Wieland, N. Peruzzi, B. Wiese, P. Heuser, J. Moosmann, A. Wennerberg, R. Willumeit-Römer, High-resolution ex vivo analysis of the degradation and osseointegration of Mg-xGd implant screws in 3D, *Bioactive Materials* (2021), doi:[10.1016/j.bioactmat.2021.10.041](https://doi.org/10.1016/j.bioactmat.2021.10.041).
- [52] R. Domander, A.A. Felder, M. Doube, BoneJ2 – refactoring established research software, (2021). <https://doi.org/10.12688/wellcomeopenres.16619.2>.
- [53] K. Donath, *Die Trenn-Dünnschliff-Technik zur Herstellung histologischer Präparate von nicht schneidbaren Geweben und Materialien: Apparate- und Methodenbeschreibung*, EXAKT-Kulzer-Druckschr., 1988.
- [54] J. Lackó, L. Géza, A simple differential staining method for semi-thin sections of ossifying cartilage and bone tissues embedded in epoxy resin, *Mikroskopie*. 31 (19750000) 1–4.
- [55] F. Witte, V. Kaese, H. Haferkamp, E. Switzer, A. Meyer-Lindenberg, C. Wirth, H. Windhagen, In vivo corrosion of four magnesium alloys and the associated bone response, *Biomaterials* 26 (2005) 3557–3563.
- [56] P.K. Bowen, J. Drelich, J. Goldman, Magnesium in the murine artery: Probing the products of corrosion, *Acta Biomaterialia* 10 (2014) 1475–1483, doi:[10.1016/j.actbio.2013.11.021](https://doi.org/10.1016/j.actbio.2013.11.021).
- [57] A. Svedbom, E. Hernlund, M. Ivergård, J. Compston, C. Cooper, J. Stenmark, E.V. McCloskey, B. Jönsson, J.A. Kanis, Osteoporosis in the European Union: a compendium of country-specific reports, *Arch Osteoporos* 8 (2013) 1–218, doi:[10.1007/s11657-013-0137-0](https://doi.org/10.1007/s11657-013-0137-0).
- [58] A. Qadir, S. Liang, Z. Wu, Z. Chen, L. Hu, A. Qian, Senile Osteoporosis: The Involvement of Differentiation and Senescence of Bone Marrow Stromal Cells, *International Journal of Molecular Sciences* 21 (2020) 349, doi:[10.3390/ijms21010349](https://doi.org/10.3390/ijms21010349).
- [59] R. Eastell, T.W. O'Neill, L.C. Hofbauer, B. Langdahl, I.R. Reid, D.T. Gold, S.R. Cummings, Postmenopausal osteoporosis, *Nat Rev Dis Primers*. 2 (2016) 16069, doi:[10.1038/nrdp.2016.69](https://doi.org/10.1038/nrdp.2016.69).
- [60] A. Varela, L. Chouinard, E. Lesage, S.Y. Smith, G. Hattersley, One Year of Abaloparatide, a Selective Activator of the PTH1 Receptor, Increased Bone Formation and Bone Mass in Osteopenic Ovariectomized Rats Without Increasing Bone Resorption, *Journal of Bone and Mineral Research* 32 (2017) 24–33, doi:[10.1002/jbmr.3003](https://doi.org/10.1002/jbmr.3003).
- [61] N. Saleh, N. Nassef, M. Shawky, M. Elshishiny, H. Saleh, Novel approach for pathogenesis of osteoporosis in ovariectomized rats as a model of postmenopausal osteoporosis, *Experimental Gerontology* 137 (2020).
- [62] E.M. Tan, L. Li, I.R. Indran, N. Chew, E.-L. Yong, TRAF6 Mediates Suppression of Osteoclastogenesis and Prevention of Ovariectomy-Induced Bone Loss by a Novel Prenylflavonoid, *Journal of Bone and Mineral Research* 32 (2017) 846–860, doi:[10.1002/jbmr.3031](https://doi.org/10.1002/jbmr.3031).
- [63] H. Zheng, S. Qi, C. Chen, Salidroside Improves Bone Histomorphology and Prevents Bone Loss in Ovariectomized Diabetic Rats by Upregulating the OPG/RANKL Ratio, *Molecules* 23 (2018) 2398, doi:[10.3390/molecules23092398](https://doi.org/10.3390/molecules23092398).
- [64] X.J. Li, W.S.S. Jee, Adaptation of diaphyseal structure to aging and decreased mechanical loading in the adult rat: A densitometric and histomorphometric study, *The Anatomical Record* 229 (1991) 291–297, doi:[10.1002/ar.1092290302](https://doi.org/10.1002/ar.1092290302).
- [65] X. Lin, D. Xiong, Y.-Q. Peng, Z.-F. Sheng, X.-Y. Wu, X.-P. Wu, F. Wu, L.-Q. Yuan, E.-Y. Liao, Epidemiology and management of osteoporosis in the People's Republic of China: current perspectives, *Clin Interv Aging* 10 (2015) 1017–1033, doi:[10.2147/CIA.S54613](https://doi.org/10.2147/CIA.S54613).
- [66] J.I. Francisco, Y. Yu, R.A. Oliver, W.R. Walsh, Relationship between age, skeletal site, and time post-ovariectomy on bone mineral and trabecular microarchitecture in rats, *Journal of Orthopaedic Research* 29 (2011) 189–196, doi:[10.1002/jor.21217](https://doi.org/10.1002/jor.21217).
- [67] A.H. Simpson, I.R. Murray, Osteoporotic Fracture Models, *Curr Osteoporos Rep* 13 (2015) 9–15, doi:[10.1007/s11914-014-0246-8](https://doi.org/10.1007/s11914-014-0246-8).
- [68] J. Wang, J. Xu, C. Hopkins, D.H. Chow, L. Qin, Biodegradable Magnesium-Based Implants in Orthopedics—A General Review and Perspectives, *Advanced Science* 7 (2020) 1902443, doi:[10.1002/adv.201902443](https://doi.org/10.1002/adv.201902443).
- [69] M. Staiger, A. Pietak, J. Huadmai, G. Dias, Magnesium and its alloys as orthopedic biomaterials: A review, *Biomaterials* 27 (2006) 1728–1734, doi:[10.1016/j.biomaterials.2005.10.003](https://doi.org/10.1016/j.biomaterials.2005.10.003).
- [70] M. Pogorielov, E. Husak, A. Solodivnik, S. Zhdanov, Magnesium-based biodegradable alloys: Degradation, application, and alloying elements, *Interventional Medicine and Applied Science* 9 (2017) 27–38, doi:[10.1556/1646.9.2017.1.04](https://doi.org/10.1556/1646.9.2017.1.04).
- [71] S. Galli, M. Stocchero, M. Andersson, J. Karlsson, W. He, T. Lilin, A. Wennerberg, R. Jimbo, The effect of magnesium on early osseointegration in osteoporotic bone: a histological and gene expression investigation, *Osteoporos Int* 28 (2017) 2195–2205, doi:[10.1007/s00198-017-4004-5](https://doi.org/10.1007/s00198-017-4004-5).
- [72] G. Li, L. Zhang, L. Wang, G. Yuan, K. Dai, J. Pei, Y. Hao, Dual modulation of bone formation and resorption with zoledronic acid-loaded biodegradable magnesium alloy implants improves osteoporotic fracture healing: An in vitro and in vivo study, *Acta Biomaterialia* 65 (2018) 486–500.
- [73] K. Pichler, S. Fischerauer, P. Ferlic, E. Martinelli, H.-P. Brezinsek, P.J. Uggowitzer, J.F. Löffler, A.-M. Weinberg, Immunological Response to Biodegradable Magnesium Implants, *JOM* 66 (2014) 573–579, doi:[10.1007/s11837-014-0874-6](https://doi.org/10.1007/s11837-014-0874-6).
- [74] T. Kraus, S.F. Fischerauer, A.C. Hänzli, P.J. Uggowitzer, J.F. Löffler, A.M. Weinberg, Magnesium alloys for temporary implants in osteosynthesis: In vivo studies of their degradation and interaction with bone, *Acta Biomaterialia* 8 (2012) 1230–1238, doi:[10.1016/j.actbio.2011.11.008](https://doi.org/10.1016/j.actbio.2011.11.008).
- [75] S. Fischerauer, T. Kraus, X. Wu, S. Tangl, E. Sorantin, A. Hänzli, J. Löffler, P. Uggowitzer, A. Weinberg, In vivo degradation performance of micro-arc-oxidized magnesium implants: A micro-CT study in rats, *Acta Biomaterialia* 9 (2013) 5411–5420, doi:[10.1016/j.actbio.2012.09.017](https://doi.org/10.1016/j.actbio.2012.09.017).
- [76] T. Kraus, S. Fischerauer, S. Treichler, E. Martinelli, J. Eichler, A. Myrissa, S. Zötsch, P. Uggowitzer, J. Löffler, A. Weinberg, The influence of biodegradable magnesium implants on the growth plate, *Acta Biomaterialia* 66 (2018) 109–117, doi:[10.1016/j.actbio.2017.11.031](https://doi.org/10.1016/j.actbio.2017.11.031).
- [77] A. Myrissa, S. Braeuer, E. Martinelli, R. Willumeit-Römer, W. Goessler, A.-M. Weinberg, Gadolinium accumulation in organs of Sprague-Dawley® rats after implantation of a biodegradable magnesium-gadolinium alloy, *Acta Biomaterialia* 48 (2017) 521–529, doi:[10.1016/j.actbio.2016.11.024](https://doi.org/10.1016/j.actbio.2016.11.024).
- [78] F. Amerstorfer, S. Fischerauer, L. Fischer, J. Eichler, J. Draxler, A. Zitek, M. Meischel, E. Martinelli, T. Kraus, S. Hann, S. Stanzl-Tschegg, P. Uggowitzer, J. Löffler, A. Weinberg, T. Prohaska, Long-term in vivo degradation behavior and near-implant distribution of resorbed elements for magnesium alloys WZ21 and ZX50, *Acta Biomaterialia* 42 (2016) 440–450, doi:[10.1016/j.actbio.2016.06.025](https://doi.org/10.1016/j.actbio.2016.06.025).
- [79] M.T. Vestermarck, J.E. Bechtold, P. Swider, K. Søballe, Mechanical interface conditions affect morphology and cellular activity of sclerotic bone rims forming around experimental loaded implants, *Journal of Orthopaedic Research* 22 (2004) 647–652, doi:[10.1016/j.orthres.2003.10.012](https://doi.org/10.1016/j.orthres.2003.10.012).
- [80] T. Yu, L. Xie, F. Chu, A Sclerotic Rim Provides Mechanical Support for the Femoral Head in Osteonecrosis, *Orthopedics* 38 (2015), doi:[10.3928/01477447-20150504-53](https://doi.org/10.3928/01477447-20150504-53).
- [81] T.R. Arnett, Extracellular pH Regulates Bone Cell Function, *The Journal of Nutrition* 138 (2008) 415S–418S, doi:[10.1093/jn/138.2.415S](https://doi.org/10.1093/jn/138.2.415S).
- [82] A. Nazarian, D. von Stechow, D. Zurakowski, R. Müller, B.D. Snyder, Bone volume fraction explains the variation in strength and stiffness of cancellous bone affected by metastatic cancer and osteoporosis, *Calcif Tissue Int* 83 (2008) 368–379, doi:[10.1007/s00223-008-9174-x](https://doi.org/10.1007/s00223-008-9174-x).
- [83] N.E. Lane, D. Haupt, D.B. Kimmel, G. Modin, J.H. Kinney, Early Estrogen Replacement Therapy Reverses the Rapid Loss of Trabecular Bone Volume and Prevents Further Deterioration of Connectivity in the Rat, *Journal of Bone and Mineral Research* 14 (1999) 206–214, doi:[10.1359/jbmr.1999.14.2.206](https://doi.org/10.1359/jbmr.1999.14.2.206).
- [84] Y. Qiu, C. Tang, M. Serrano-Sosa, J. Hu, J. Zhu, G. Tang, C. Huang, M. Huang, Bone microarchitectural parameters can detect oxytocin induced changes prior to bone density on mitigating bone deterioration in rabbit osteoporosis model using micro-CT, *BMC Musculoskelet Disord* 20 (2019) 560, doi:[10.1186/s12891-019-2861-0](https://doi.org/10.1186/s12891-019-2861-0).
- [85] Y. Wu, S. Adee, M.R. Doschak, Using Micro-CT Derived Bone Microarchitecture to Analyze Bone Stiffness - A Case Study on Osteoporosis Rat Bone, *Front Endocrinol (Lausanne)* 6 (2015) 80, doi:[10.3389/fendo.2015.00080](https://doi.org/10.3389/fendo.2015.00080).